Research Article
Malays. j. med. biol. res.

Structural Analysis of $NaYF_4$ Solution Processed Nanoparticles for Hela Cell Studies

Cliff Orori Mosiori[1*], John Maera[2]

[1]Department of Mathematics and Physics, Technical University of Mombasa, P. O. Box 90420, Mombasa, **KENYA**
[2]Department of Mathematics and Physical Sciences, Maasai Mara University, P. O. Box 420, Narok, **KENYA**

[*]Email for Correspondence: corori@tum.ac.ke

ABSTRACT

The $NaYF_4$ nanoparticles were prepared and analyzed. Its structural analysis confirmed the formation of nanocrystals of desired sizes and spectral properties that can be incorporated into Hela cell studies. Internalization of $NaYF_4$ nanoparticles in HeLa cells were determined at different nanoparticles concentrations and for incubation periods from 3 to 24 hours using various techniques. The images revealed a redistribution of nanoparticles inside the cell that increased with incubation time, concentration levels and depended on the presence of the transfection factor. The study identified factors responsible for an effective endocytosis of the $NaYF_4$ nanoparticles to HeLa cells. Thus this procedure or method could be applied to investigate a wide range of future "smart" theranostic agents that may result into be very promising fluorescent probes for imaging real-time cellular dynamics.

Keywords: lanthanide, nanocrystal, polyvinylpyrrolidone, HeLa cell, incubation, endocytosis

4/28/2020 **Source of Support:** Nil, **No Conflict of Interest:** Declared

INTRODUCTION

Rapid advances of nanotechnology have led to the development of new unique nanoparticles that emit light after excitation with NIR energy. Reducing nanoparticles size has stimulated its inclusion into enhanced cellular penetration. This allowed intracellular imaging applications in photodynamic therapy (Manikandan et al., 2014). Particles in the Quantum dots size (Hill & Howard, 1987) and metallic nanoparticles levels (Peters et al., 2014) have been extensively studied as two-photon fluorescent biomarkers in living cells and other biological applications. Two-photon emission spectra obtained using NIR excitation indicate that it strongly depends on the shape of the nanocrystals involved and its environment. There is an ongoing need for research on new materials to help in overcoming various problems associated with toxicity. *In vivo* imaging using a UV visible radiation has shown several disadvantages. It has a small penetration depth into the tissue, and the possibility of damaging the sample under test (Leite et al., 2002). Therefore, Biophysicist has proposed the "single photon" fluorescent that emits a low energy photon as a result of a higher energy photon absorption in UV range. The use of femtosecond pulses permits to reduce the thermal load causing tissue damage (Walter et al., 2014; Karpov et al., 2014). Using this technology, its sensitivity and resolution can be improved when "multiphoton" process and near-infrared light (NIR) is applied to excite the samples under test. Therefore, the use of near-infrared (NIR) radiation within the "optical transmission window" (780 - 1200 nm) of biological tissues has many advantages. These can be listed as an increase of optical contrast, a greater depth of light penetration, minimized auto-fluorescence and even a reduced light scattering (Hill & Howard, 1987). Its established that, NIR radiation does not cause damage to cellular functions and structures (Manikandan et al., 2014) and thus by reducing the damage will allows bio-dynamical imagining. This is a technique that requires long duration of exposure to the (NIR) irradiation hence showing efficient and stable optical conversion of multiphoton fluorescence,

after excitation by femtosecond NIR. These are suitable for imaging of the time-dependent intracellular processes (Kumar Srivastav et al., 2013). Several literature reports have described $NaYF_4$ nanocrystals of various shapes and sizes (Leite et al., 2002). An important factor is the choice of the host material which should have the crystal structure matched to ion-doped and low phonon energy to minimize non-radiative relaxation processes and to maximize radiative emission. It's proposed that $NaYF_4$ crystals can satisfy those mentioned criterion (Manikandan et al., 2014). Therefore, this paper reports the investigation on the concentration of the absorber (Yb^{3+} dopant ions) in order to maximize efficiency.

MATERIALS AND METHODS

Growth and Synthesis of $NaYF_4$ nanoparticles

All reagents used were bought from Sigma-Aldrich. To obtain $NaYF_4$ various amounts of Er^{3+}, Yb^{3+} nanoparticles were synthesized whereby Y_2O_3 (1-x mmol), Yb_2O_3 (x mmol, where x = 0.1; 0.18; 0.2; 0.3 mmol and 0.02 mmol) was dissolved in 10% HNO_3 (10 ml). After complete reaction, it was heated to evaporate water. Thereafter, ethylene glycol (10 ml) was added to dissolve the obtained rare Y- earth nitrate. Polyvinylpyrrolidone - PVP40 (0.556 g) and NaCl (1 mmol) was added and the solution was then heated to 80 °C until a homogeneous solution. Finally, NH_4F (4 mmol) was dissolved in ethylene glycol (10 ml) at 80 °C and then added drop wise to a solution of nitrate.

Preparation of $NaYF_4$ into HeLa scientific cells

HeLa is a cell type in an immortal cell line used in scientific research. In this study, a sample of the HeLa cells was bought from Sigma Aldrich suppliers. Cells were cultured in 6 well plates dishes (6 x 10 cm^2) at a density of 100 000 / plate. Cultures of cells were kept at 37 °C in a humidified atmosphere containing 5% CO_2. 10 µl of sonicated initial colloidal solution of $NaYF_4$ in water was dissolved in 500 µl H_2O mixed and incubated for 20 minutes. Lipofectamine 2000 was used to introduce $NaYF_4$ nanoparticles into the cells. 20µl Lipofectamine 2000 was dissolved in 500µl miliR H_2O and incubated for 15 minutes. They were then incubated together. 500 µl of this solution was added to 10 cm^2 dish with HeLa cells and incubated at different times. Then different sets of variables were tested the incubation times of 3 h, 6 h, 12 h and 24 h; concentration of nanoparticles: 0.2 µM, 0.4 µM, 2.0 µM, 4.0 µM, 20 µM and 40 µM respectively.

Characterization of $NaYF_4$ nanoparticles

The crystal structure was determined using the Philips X´Pert Pro Alpha1 MPD diffractometer in the range of 2θ (10° - 150°) for 15 hours while the size of the crystals was determined a full width half maximum (FWHM) using the Scherrer formula by using Fullprof. TEM measurements were performed in methanol dispersion while surface morphology was analyzed by Auriga - Zeiss field emission scanning electron microscopy (FE-SEM). Elemental analysis was done using QUANTAX 400 Bruker Energy-dispersive X-ray spectroscopy system while the fluorescence spectrum was measured with a 960 nm continues wave (CW) laser diode with 194 mW power and CCD detection (Spex 270M).

Characterization treated HeLa scientific cells

The HeLa cells were analyzed using a Zeiss 710 NLO fluorescence confocal microscope with a NIR femtosecond laser by observing two channels: one with excitation 980 nm (femtosecond laser) and emission range from 515 to 671 nm; the second with excitation 488 nm (continues wave CW) and emission range from 508 to 585 nm and the data analyzed by CellProfiler program.

RESULTS AND DISCUSSION

$NaYF_4$ nanoparticles were characterized using the Transmission Electron Microscopy (TEM), X-ray diffraction, and photoluminescence and then they were introduced to HeLa cells and luminescence was observed. The impact of incubation time and its distribution inside cells was examined. Lipofectamine 2000 was used a transfection factor was applied in order to improve the efficiency of nanoparticles uptake into cells. The distribution of $NaYF_4$ nanoparticles, as a function of incubation time and concentration in the presence and absence of the cellular transporter, was analyzed inside HeLa cells.

Structural characterization of $NaYF_4$ nanoparticles

X-ray diffraction data obtained were consistent with cubic structured $NaYF_4$ nanocrystals confirming that the literature on obtaining similar mixtures of cubic and hexagonal $NaYF_4$ nanocrystals (Manikandan et al., 2014). It was concluded that the method and conditions used in this study were accurate. The size of the nanocrystals evaluated from the Scherrer formula (Gavrilović et al., 2014) ranged from 30 nm for nanoparticles.

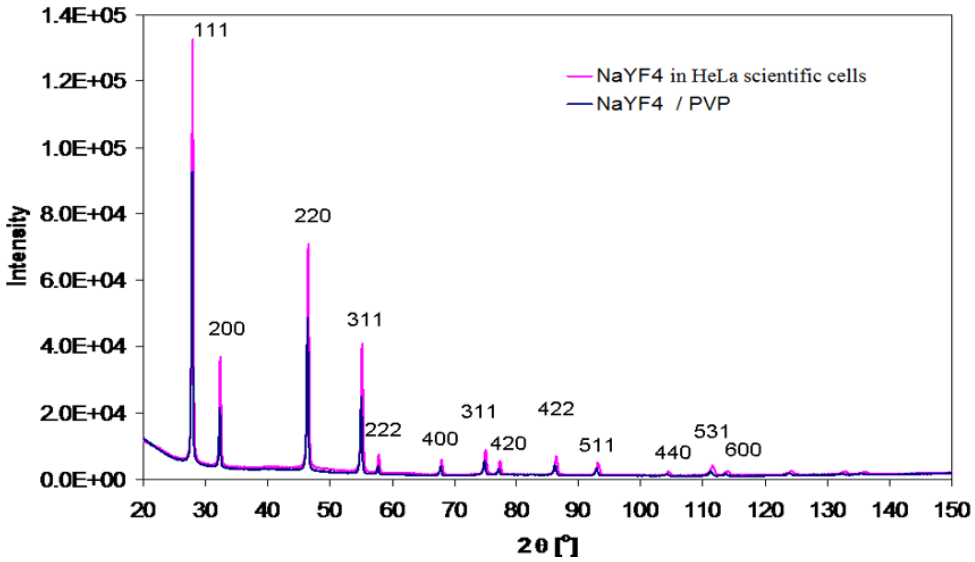

Figure 1: X-ray diffraction pattern of $NaYF_4$ nanoparticles

$NaYF_4$ lattice constant was obtained from calculations using the data from the XRD (Basith et al., 2014). Its lattice constants were calculated using the Rietveld method. As a result $NaYF_4$ network the lattice parameters changed from 5.52 Å to 5.51 Å as illustrated in figure 2. However, no visible change of lattice constant depending on the content of ytterbium was observed. The lattice constant obtained for $NaYF_4$ nanoparticles without dopant was 5.518 and this was greater than that of bulk crystal as published in the JCPDS card (No. 77-2042, a = 5.470 Å). Similar results are reported in stresses in lattice in the nanocrystals than in bulk materials (Karpov et al., 2014).

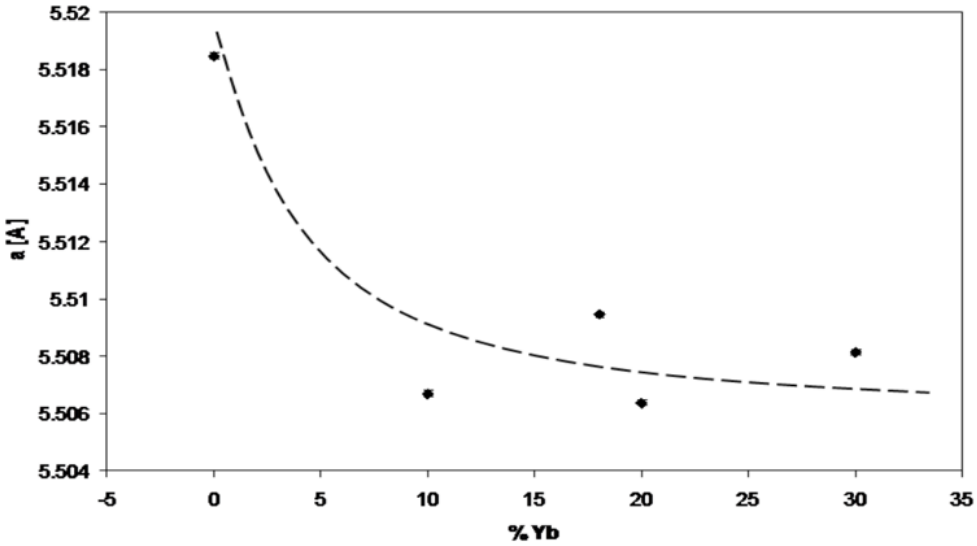

Figure 2. $NaYF_4$ lattice constant obtained from calculations

Elemental EDX characterization of $NaYF_4$ nanoparticles

Elemental EDX analysis of $NaYF_4$ nanoparticles was performed for all of the nanoparticles samples and obtained as: ions (Yb^{3+}) to ions (Er^{3+}) was about 11.2 ratio F^{3+}/Y^{3+} ~ 5.6 Y^{3+}/Er^{3+} ~ 31.6 Y^{3+}/Yb^{3+} ~ 2.7 Y^{3+}/Na^{3+} ~ 1.3; F^{3+}/Na^{3+} ~ 6.2 respectively. The results showed that the reaction ratios agree with the ratios obtained from the quantitative EDX analysis (Ebrahimi et al., 2014; Walter et al., 2014).

TEM characterization of $NaYF_4$ nanoparticles

TEM images of $NaYF_4$ nanoparticles showed a well-defined crystal structure as depicted in figure 4 that was polyhedral in shape and uniform in size with average size around 30 nm. The apparent size differences were statistically insignificant based on 100-160 individual nanostructures per sample TEM determinations. Black areas spotted in the figure 4 were attributed to burned spots during the electron beam exposure during TEM measurements.

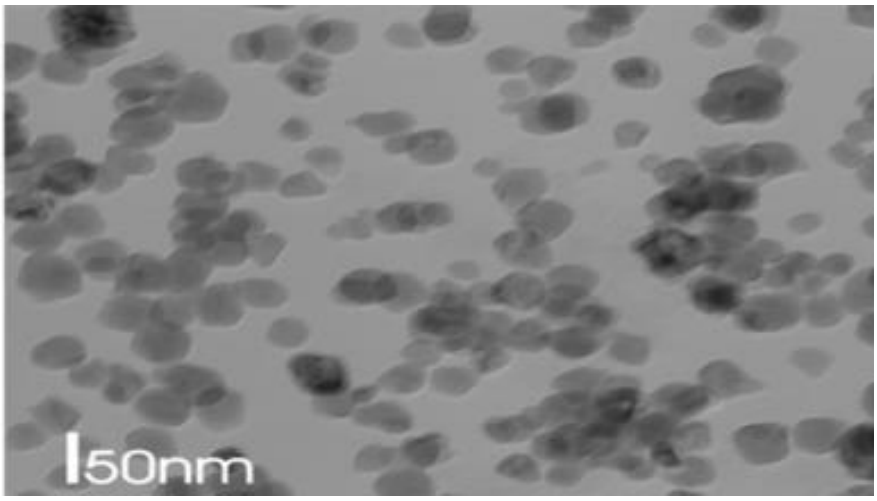

Figure 4: Transmission electron microscope image

Luminescence characterization of $NaYF_4$ nanoparticles

Only ions incorporated in the crystal lattice were analyzed using Rietveld method based on X-ray diffraction measurements. Rietveld refinements showed that the Y^{3+} site was partially occupied by Yb^{3+} ions. All Er^{3+} ions occupied the Y^{3+} sites (Leite et al., 2002; Kumar Srivastav et al., 2013). These calculations provided Yb^{3+} fractional occupancy lower than the technological fraction from pure $NaYF_4$ nanoparticles A linear dependence of luminescence intensity versus Yb^{3+} occupancy obtained and illustrated figure 3 supports the expectation that only site-located Yb^{3+} ions contribute to luminescence.

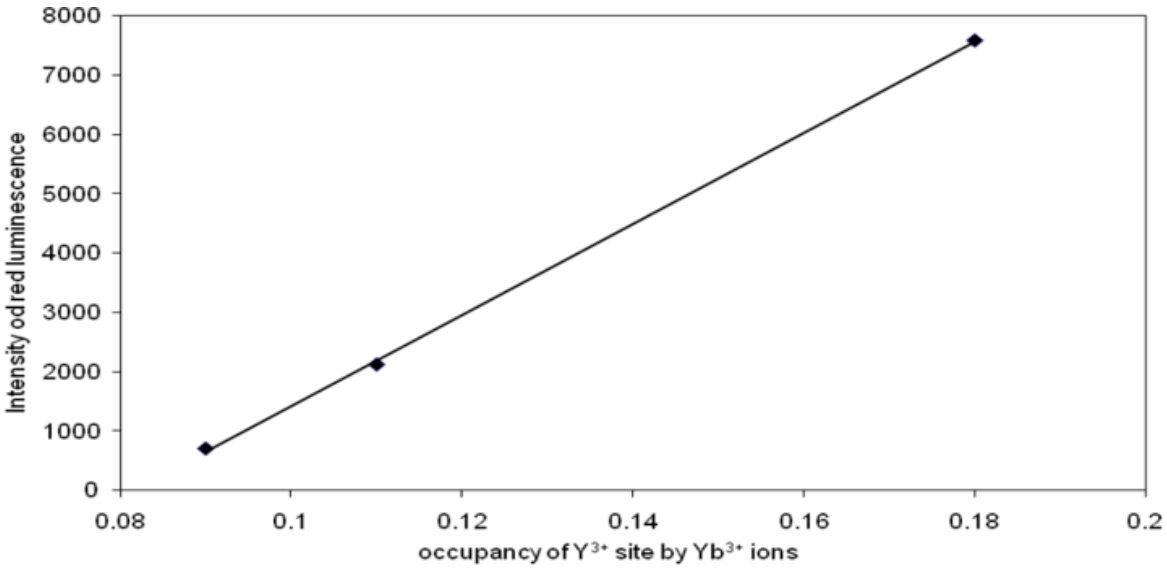

Figure 3: Luminescence intensity on Y^{3+} sites by Yb^{3+} ions

Fluorescence spectra showed emission peaks at 522, 541 and 652 nm are the result from $^4H_{11/2}$, $^4S_{3/2}$, $^4F_{9/2}$ to $^4I_{15/2}$ transition of Er^{3+}ions, respectively (Leite et al., 2002). The bands did not depend on the size of nanoparticles but were found to can change the intensity of the fluorescence peaks of the ions. For nanoparticles $NaYF_4$ strong red fluorescence was observed (Kumar Srivastav et al., 2013) where the ratio of red to green luminescence changes depend on the amount of ions of ytterbium in lattice crystal. This agrees with the amount of ions in a lattice crystal designated from the Rietveld method (Ebrahimi et al., 2014; Di Giovanni, 2014). Fluorescent bands showed a well-defined structure as opposed to the fluorescent bands generated by quantum dots (Peters et al., 2014) or gold nanoparticles. This was attributed to simultaneous emission of the different close electron energy levels of Er^{3+} ions. The emission bands were narrower than the quantum dots (Hameed et al., 2014) or gold nanoparticles (Young et al., 1993) resulting in higher contrast images through better spectral distinction from the auto fluorescence of cells. These advantages make $NaYF_4$ nanoparticles excellent candidates for the next generation of nanoprobes for *in vivo* bioluminescence imaging.

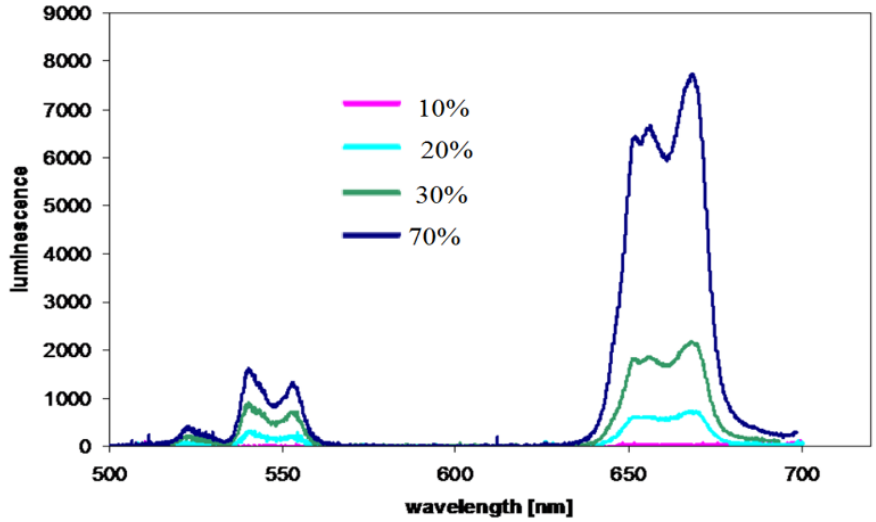

Figure 6: Fluorescence spectra of $NaYF_4$

HeLa cells with $NaYF_4$ nanoparticles

Aqueous suspensions of $NaYF_4$ nanoparticles were introduced into the HeLa cancer cells by simple incubation to obtain high-contrast two-photon fluorescence (Grujić-Brojčin et al., 2014). The results demonstrated that for short incubation times, $NaYF_4$ nanoparticles were homogeneously distributed inside the cell (Young et al., 1993).while for longer incubation times, the spatial distribution of $NaYF_4$ nanoparticles were highly inhomogeneous (Manikandan et al., 2014). Images of single cells were obtained after different incubation times whereby confocal images of HeLa cells after 3 h, 6 h, 12 h and 24 h incubation showed that prolonged incubation time, increased quantities of nanoparticles inside the HeLa cells (figure 8). On the other hand, for longer incubation times (24 h with and 24 h without the vesicles) nanoparticles were mainly localized in the vicinity of the nucleus. This was attributed to the spatial redistribution of the nanoparticles is caused by the transport of nutrients from the cell membrane to the vicinity of the cell nucleus (Riwotzki et al., 2001).

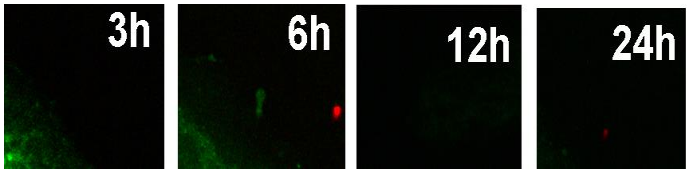

Figure 7: Confocal images of HeLa cells after 3 h, 6 h, 12 h and 24 h incubation times.

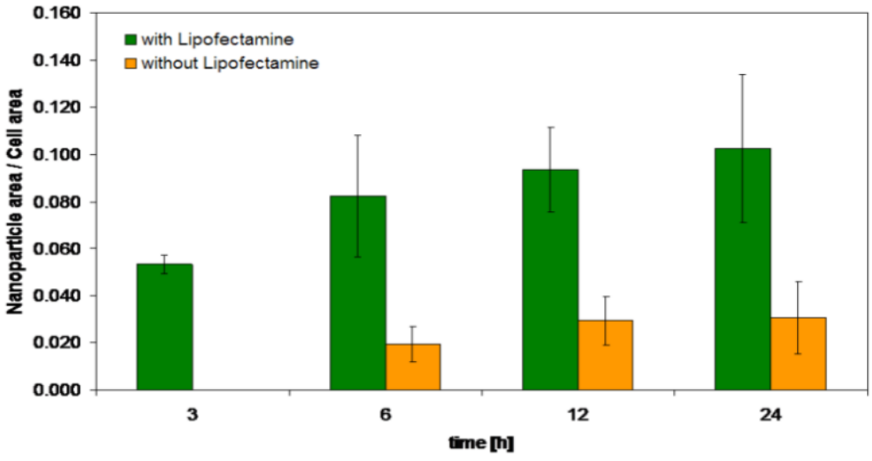

Figure 8: The ratios indifferent incubation time as analyzed by CellProfiler program

It has been observed that when the concentration of nanoparticles increases by 10 times, some nanoparticles appear in the cytoplasm inside cells. In the case of nanoparticles incubated with cells in the presence of Lipofectamine 2000 much more nanoparticles enter into cells (Maiyalagan et al., 2014) in comparison to incubation without Lipofectamine 2000.

CONCLUSIONS

Small, pure cubic phase $NaYF_4$ nanoparticles were synthesized using PVP as a chelating agent. These nanoparticles were uniform and their size varied depending on the experimental conditions. The crystals were monodisperse in water and images of single cells obtained after different incubation times and with or without the liposomes showed the varied dynamic behavior inside the cell. Incubation with the liposomes causes enhanced incorporation of nanoparticles. This result presents an evidence of potential applications of $NaYF_4$ nanoparticles to static and dynamic bioimaging. Similar observations were made based on the nanoparticles concentration dependent study in the presence and absence of the transporter. It was then concluded that a good selection of nanoparticles concentration and time of incubation has critical influence on the fabrication and development of multimodal imagining materials.

ACKNOWLEDGEMENTS

We acknowledge Prof. Grzegorz of NIEB Academy of Science for performing confocal microscopy measurements and Dr, Pawełnel Kraw for performing the Cellprofiler analysis.

REFERENCES

Basith, N. M., Vijaya, J. J., Kennedy, L. J., Bououdina, M., Jenefar, S., & Kaviyarasan, V. (2014). Co-doped ZnO nanoparticles: structural, morphological, optical, magnetic and antibacterial studies. *Journal of Materials Science & Technology*, *30*(11), 1108-1117.

Di Giovanni, C., Wang, W. A., Nowak, S., Grenèche, J. M., Lecoq, H., Mouton, L., ... & Tard, C. (2014). Bioinspired iron sulfide nanoparticles for cheap and long-lived electrocatalytic molecular hydrogen evolution in neutral water. *Acs Catalysis*, *4*(2), 681-687.

Ebrahimi, S. S., Masoudpanah, S. M., Amiri, H., & Yousefzadeh, M. (2014). Magnetic properties of MnZn ferrite nanoparticles obtained by SHS and sol-gel autocombustion techniques. *Ceramics International*, *40*(5), 6713-6718.

Gavrilović, T. V., Jovanović, D. J., Lojpur, V., & Dramićanin, M. D. (2014). Multifunctional $Eu^{3+}$and Er^{3+}/Yb^{3+}-doped $GdVO_4$ nanoparticles synthesized by reverse micelle method. *Scientific reports*, *4*, 4209.

Grujić-Brojčin, M., Armaković, S., Tomić, N., Abramović, B., Golubović, A., Stojadinović, B., ... & Šćepanović, M. (2014). Surface modification of sol–gel synthesized TiO 2 nanoparticles induced by La-doping. *Materials Characterization*, *88*, 30-41.

Hameed, A. S., Bahiraei, H., Reddy, M. V., Shoushtari, M. Z., Vittal, J. J., Ong, C. K., & Chowdari, B. V. R. (2014). Lithium storage properties of pristine and (Mg, Cu) codoped ZnFe2O4 nanoparticles. *ACS applied materials & interfaces*, *6*(13), 10744-10753.

Hill, R. J., & Howard, C. J. (1987). Quantitative phase analysis from neutron powder diffraction data using the Rietveld method. *Journal of Applied Crystallography*, *20*(6), 467-474.

Karpov, I., Ushakov, A., Fedorov, L., & Lepeshev, A. (2014). Method for producing nanomaterials in the plasma of a low-pressure pulsed arc discharge. *Technical Physics*, *59*(4).

Kumar Srivastav, S., Gajbhiye, N. S., & Banerjee, A. (2013). Structural transformation and enhancement in magnetic properties of single-phase Bi1− xPrxFeO3 nanoparticles. *Journal of Applied Physics*, *113*(20), 203917.

Leite, E. R., Maciel, A. P., Weber, I. T., Lisboa-Filho, P. N., Longo, E., Paiva-Santos, C. O., ... & Schreiner, W. H. (2002). Development of metal oxide nanoparticles with high stability against particle growth using a metastable solid solution. *Advanced Materials*, *14*(12), 905-908.

Maiyalagan, T., Jarvis, K. A., Therese, S., Ferreira, P. J., & Manthiram, A. (2014). Spinel-type lithium cobalt oxide as a bifunctional electrocatalyst for the oxygen evolution and oxygen reduction reactions. *Nature communications*, *5*.

Manikandan, A., Kennedy, L. J., Bououdina, M., & Vijaya, J. J. (2014). Synthesis, optical and magnetic properties of pure and Co-doped $ZnFe_2O_4$ nanoparticles by microwave combustion method. *Journal of Magnetism and Magnetic Materials*, *349*, 249-258.

Manikandan, A., Vijaya, J. J., Mary, J. A., Kennedy, L. J., & Dinesh, A. (2014). Structural, optical and magnetic properties of Fe_3O_4 nanoparticles prepared by a facile microwave combustion method. *Journal of Industrial and Engineering Chemistry*, *20*(4), 2077-2085.

Peters, R. J., van Bemmel, G., Herrera-Rivera, Z., Helsper, H. P., Marvin, H. J., Weigel, S., ... & Bouwmeester, H. (2014). Characterization of titanium dioxide nanoparticles in food products: analytical methods to define nanoparticles. *Journal of agricultural and food chemistry*, *62*(27), 6285-6293.

Riwotzki, K., Meyssamy, H., Schnablegger, H., Kornowski, A., & Haase, M. (2001). Liquid-Phase Synthesis of Colloids and Redispersible Powders of Strongly Luminescing $LaPO_4$:Ce,Tb Nanocrystals. *Angewandte Chemie International Edition*, *40*(3), 573-576.

Walter, A., Billotey, C., Garofalo, A., Ulhaq-Bouillet, C., Lefèvre, C., Taleb, J., ... & Gazeau, F. (2014). Mastering the shape and composition of dendronized iron oxide nanoparticles to tailor magnetic resonance imaging and hyperthermia. *Chemistry of Materials*, *26*(18), 5252-5264.

Young, D. S., Sachais, B. S., & Jefferies, L. C. (1993). The rietveld method.

--0--